Propulsion of a Swimming Micro Medical Robot

Gábor Kósa and Moshe Shoham
Faculty of Mechanical Engineering
Technion, Israel Institute of Technology
Technion City, 32000 Haifa, Israel
mekosha@tx.technion.ac.il

Menashe Zaaroor
Department of Department of Neurosurgery Haifa, Israel
Rambam Medical Center
Haifa, Israel
nicedoc@walla.co.il

***Abstract* – Medical doctors use radiology, endoscopy and smart pills to inspect the human body's inner content. Nowadays, self-propelled micro robots are developed to fulfill these tasks which use types of crawling techniques to advance. This paper suggests a novel swimming method, which creates a traveling wave in an elastic tail made of piezo-electric actuators, for propulsion of a micro-robot in the body. The novel swimming method was analyzed and optimized analytically by solving the coupled elastic/fluidic problem. It was found that under the extreme size limitations a tail manufactured by current MEMS technology is able to swim at the order of several mm/sec in water.**

Index Terms – Micro Robot, Medical Robot, Fluid Flow Analysis, Swimming Robot.

I. Introduction

The ideal micro robot for medical applications is a totally autonomous one that incorporates a control unit, power source, positioning and maneuvering actuators, and is able to freely navigate and perform medical procedures within the human body (see [1] for classification of micro robots). Such a system is on the verge of "science fiction" but several micro medical devices have already been developed that posses some robotics aspects such as micro catheters [2], smart pills [3] and swimming micro robots [4]. In this investigation we concentrate on micro-robots with swimming ability since they can be used for next generation un-tethered endoscopes that transmit images from inside the body. Other potential uses of such micro-robots are treatment of a specific location [5] and local drug delivery [6], the propulsion of such micro-robots is treated in [7-9].

When dealing with miniaturization, it is not possible to downscale a macro propulsion systems such as propeller or jet even though the components of such a unit have been already developed (probably this is one of the reasons that bacteria have not used the propeller). The need for a new propulsion concept is due to the nature of the flow in small scales. A micro robot of a typical dimension of 1 mm, velocity of 1 mm/sec that swims in water has Reynolds number of 1. Hence, the viscosity has much larger affect and the flow should be analyzed by Stokes equation.

This investigation proposes to propel a micro-robot by tails built of piezoelectric actuators (See Fig. 1) where the propulsion is achieved by creating a traveling wave in the tail. In contrast to macro size swimmers standing waves can't advance a micro robot in Stokes flow.

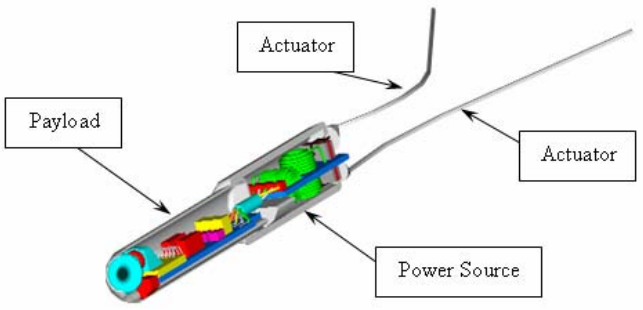

Fig. 1: Illustration of an un-tethered swimming micro-robot.

II. Propulsion Model

Fig. 1 illustrates the concept a micro-robot propelled by elastic tails. Each tail is actuated by 3 piezoelectric actuators, that are modeled as Euler-Bernoulli beam. The beam is divided into three parts each has it own elastic fields (See Fig. 2) defined as follows:

$$\begin{aligned}
&\mathsf{m}_1 \frac{\partial^2 w_1(x,t)}{\partial t^2} + c_1 \frac{\partial w_1(x,t)}{\partial t} + \hat{\mathsf{K}}_1 \frac{\partial^4 w_1(x,t)}{\partial x^4} = 0 \forall x = [0, \alpha_1 L] \\
&\mathsf{m}_2 \frac{\partial^2 w_2(x,t)}{\partial t^2} + c_2 \frac{\partial w_1(x,t)}{\partial t} + \hat{\mathsf{K}}_2 \frac{\partial^4 w_2(x,t)}{\partial x^4} = 0 \forall x = [\alpha_1 L, \alpha_2 L] \\
&\mathsf{m}_3 \frac{\partial^2 w_3(x,t)}{\partial t^2} + c_3 \frac{\partial w_1(x,t)}{\partial t} + \hat{\mathsf{K}}_3 \frac{\partial^4 w_3(x,t)}{\partial x^4} = 0 \forall x = [\alpha_1 L, L]
\end{aligned} \quad (1)$$

where: $\mathsf{m}_i = \sum_{j=1}^{n} \rho_{ij} A_{ij}$ is the distributed mass;

$\hat{\mathsf{K}}_i = \sum_{j=1}^{n} Y_j [(1+\xi_j) I_j + A_j Z_j^2]$ is the stiffness coefficient, with correction term due to the weakening of the electric field applied on the piezoelectric layers ξ_j by the cross coupling [10];

$$c_i = \frac{2\mu\kappa K_1(\kappa a_i)((K_2(\kappa a_i)K_0(\kappa a_i) - K_1^2(\kappa a_i))\kappa a_i - 4K_1(\kappa a_i)K_2(\kappa a_i)}{((K_2(\kappa a_i) + K_0(\kappa a_i))K_1^2(\kappa a_i) - 2K_0^2(\kappa a_i)K_2(\kappa a_i))\kappa a_i + 2K_2(\kappa a_i)K_0(\kappa a_i)K_1(\kappa a_i)}$$

is the damping coefficient based modified Bessel functions of the (κ is the wave number and a is the radius of the tail) in viscous fluid assuming that the flow around the tail is a Stokes flow and the amplitude of the travelling wave is small, i.e. the deformed cross section of the tail remains circular [10].

Fig. 2: The tail's three sections.

The boundary conditions of the beam are clamped at $x = 0$ and free at $x = L$:

$$\begin{array}{ll} @x=0 & @x=L \\ w_1(0,t)=0 & M_3(L,t)=0 \\ \dfrac{\partial w_1(0,t)}{\partial x}=0 & \dfrac{\partial M_3(L,t)}{\partial x}=0 \end{array} \quad ; \quad .(2)$$

The continuity conditions between the elastic fields are:

$$\begin{array}{ll} @x=\alpha_1 L & @x=\alpha_2 L \\ w_1(\alpha_1 L,t)=w_2(\alpha_1 L,t) & w_2(\alpha_1 L,t)=w_3(\alpha_1 L,t) \\ \dfrac{\partial w_1(\alpha_1 L,t)}{\partial x}=\dfrac{\partial w_2(\alpha_1 L,t)}{\partial x} & \dfrac{\partial w_2(\alpha_2 L,t)}{\partial x}=\dfrac{\partial w_3(\alpha_2 L,t)}{\partial x} \\ M_1(\alpha_1 L,t)=M_2(\alpha_1 L,t) & M_2(\alpha_2 L,t)=M_3(\alpha_2 L,t) \\ \dfrac{\partial M_1(\alpha_1 L,t)}{\partial x}=\dfrac{\partial M_2(\alpha_1 L,t)}{\partial x} & \dfrac{\partial M_2(\alpha_2 L,t)}{\partial x}=\dfrac{\partial M_3(\alpha_2 L,t)}{\partial x} \end{array} \quad ; \quad .(3)$$

Following [11], the moment M_i in a piezoelectric layered beam is calculated as follows:

$$M_i(x,t)=-\hat{K}_i\frac{\partial^2 w_i(x,t)}{\partial x^2}-M_{Ei}(t)\;\forall i=1,2,3 \qquad (4)$$

$M_{Ei}(t)$ are the moments that are created in the beam by the electric field.

As a result, the boundary (BC) and continuity conditions (CC) become inhomogeneous. We used a polynomial transformation to convert the variable $w_i(x,t)$ and create homogeneous BC and CC. This transformation enables solving the elastic field equation by separation of variables. The transformed field equation is:

$$\begin{aligned} &m_1\frac{\partial^2 z_1(x,t)}{\partial t^2}+c_1\frac{\partial z_1(x,t)}{\partial t}+\hat{K}_1\frac{\partial^4 z_1(x,t)}{\partial x^4}=\frac{p_1(x)}{\hat{K}_1}\left(\frac{m_1 d^2 M_{E1}(t)}{dt^2}+\frac{c_1 dM_{E1}(t)}{dt}\right) \\ &\forall x=[0,\alpha_1 L] \\ &m_2\frac{\partial^2 z_2(x,t)}{\partial t^2}+c_2\frac{\partial z_2(x,t)}{\partial t}+\hat{K}_2\frac{\partial^4 z_2(x,t)}{\partial x^4}=\frac{p_2(x)}{\hat{K}_1}\left(\frac{m_2 d^2 M_{E1}(t)}{dt^2}+\frac{c_2 dM_{E1}(t)}{dt}\right) \\ &+\frac{p_3(x)}{\hat{K}_2}\left(\frac{m_2 d^2 M_{E2}(t)}{dt^2}+\frac{c_2 dM_{E2}(t)}{dt}\right)\forall x=[\alpha_1 L,\alpha_2 L] \\ &m_3\frac{\partial^2 z_3(x,t)}{\partial t^2}+c_3\frac{\partial z_3(x,t)}{\partial t}+\hat{K}_3\frac{\partial^4 z_3(x,t)}{\partial x^4}=\frac{p_4(x)}{\hat{K}_1}\left(\frac{m_3 d^2 M_{E1}(t)}{dt^2}+\frac{c_3 dM_{E1}(t)}{dt}\right) \\ &+\frac{p_5(x)}{\hat{K}_2}\left(\frac{m_2 d^2 M_{E2}(t)}{dt^2}+\frac{c_2 dM_{E2}(t)}{dt}\right)+\frac{p_6(x)}{\hat{K}_3}\left(\frac{m_3 d^2 M_{E3}(t)}{dt^2}+\frac{c_3 dM_{E3}(t)}{dt}\right) \\ &\forall x=[\alpha_1 L,L] \end{aligned} \qquad (5)$$

The polynoms $p_i(x)$ form three polynoms along the tail shown in Fig. 3.

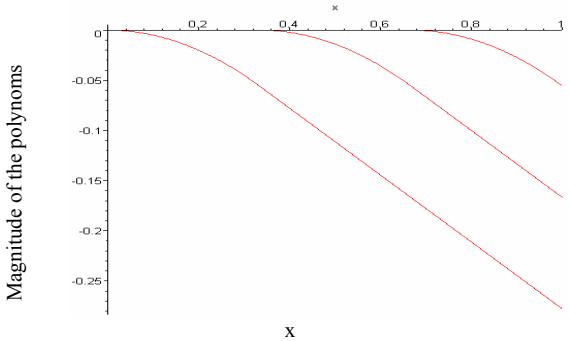

Fig. 3: Illustration of the polynoms for $L=1;\alpha_1=1/3;\alpha_2=2/3$.

The general solution of (3) is given by:

$$z_i(x,t)=\sum_k^{\infty}\phi_{i,k}(x)f_k(t)\;\forall i=1,2,3 \qquad (6)$$

where: $f_k(t)$ - are the time functions of the variable separation. This function is the same in the different elastic fields along the tail.

$\phi_{i,k}(x)$ - are the shape modes of the system.

The modes differ at each elastic field, but the continuity conditions ensure that they create a smooth spatial function along the three parts of the beam.

By substituting the general solutions, (6), into the BC and CC one can find the natural frequencies and the mode shapes of the beam. Fig. 4 illustrates the first 4 modes of the tail ($m_i=m;K_i=K$).

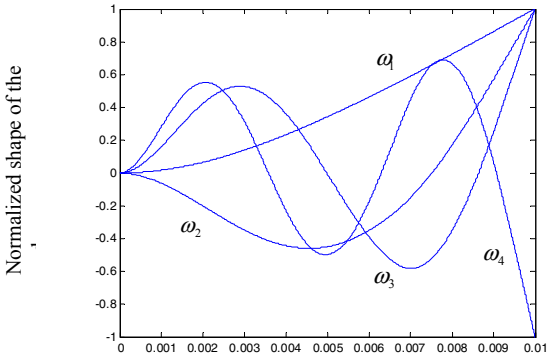

Fig. 4: The beams' modes.

The polynoms shown in Fig 3 are decomposed into the beam's modes and enables deriving the evolution equations of each mode:

$$\begin{aligned} &\ddot{f}_k(t)+2\zeta_{1k}\omega_k\dot{f}_k(t)+\omega_k^2 f_k(t)=\frac{Cp_k^{(1)}}{\hat{K}_1}\left(\ddot{M}_{E1}(t)+2\zeta_{1k}\omega_k\dot{M}_{E1}(t)\right) \\ &\ddot{f}_k(t)+2\zeta_{2k}\omega_k\dot{f}_k(t)+\omega_k^2 f_k(t)=\frac{Cp_k^{(1)}}{\hat{K}_1}\left(\ddot{M}_{E1}(t)+2\zeta_{2k}\omega_k\dot{M}_{E1}(t)\right) \\ &+\frac{Cp_k^{(2)}}{\hat{K}_2}\left(\ddot{M}_{E2}(t)+2\zeta_{2k}\omega_k\dot{M}_{E2}(t)\right) \\ &\ddot{f}_k(t)+2\zeta_{3k}\omega_k\dot{f}_k(t)+\omega_k^2 f_k(t)=\frac{Cp_k^{(1)}}{\hat{K}_1}\left(\ddot{M}_{E1}(t)+2\zeta_{3k}\omega_k\dot{M}_{E1}(t)\right) \\ &+\frac{Cp_k^{(2)}}{\hat{K}_2}\left(\ddot{M}_{E2}(t)+2\zeta_{3k}\omega_k\dot{M}_{E2}(t)\right) \\ &+\frac{Cp_k^{(3)}}{\hat{K}_3}\left(\ddot{M}_{E3}(t)+2\zeta_{2k}\omega_k\dot{M}_{E3}(t)\right)\forall k=1,2,..\infty \end{aligned} \qquad (7)$$

$Cp_k^{(i)}$ - is a constant derived by the decomposition of the polynomial $p_i(x)$ to the k-th shape function $\phi_k(x)$.

In order to find the general behaviour of the beam one has to calculate the contribution of each moment, $M_{Ei}(t)$, separately, and the total time response is the superposition:

$$f_k=\sum_{i=1}^{3}f_k^{(i)} \qquad (8)$$

Converting to the Laplace domain and substituting into (8) the transformation between the moments M_{Ei} and the time functions, $f_k(t)$ is:

$$f_k = -\frac{Cp_k^{(1)}\mathsf{M}_{E1}}{\hat{\mathsf{K}}_1}\left(\frac{s(s+2\zeta_{1k}\omega_k)}{s^2+2\zeta_{1k}\omega_k s+\omega_k^2}+\frac{s(s+2\zeta_{2k}\omega_k)}{s^2+2\zeta_{2k}\omega_k s+\omega_k^2}+\frac{s(s+2\zeta_{3k}\omega_k)}{s^2+2\zeta_{3k}\omega_k s+\omega_k^2}\right) \quad (9)$$
$$-\frac{Cp_k^{(2)}\mathsf{M}_{E2}}{\hat{\mathsf{K}}_2}\left(\frac{s(s+2\zeta_{2k}\omega_k)}{s^2+2\zeta_{2k}\omega_k s+\omega_k^2}+\frac{s(s+2\zeta_{3k}\omega_k)}{s^2+2\zeta_{3k}\omega_k s+\omega_k^2}\right)$$
$$-\frac{Cp_k^{(3)}\mathsf{M}_{E3}}{\hat{\mathsf{K}}_2}\frac{s(s+2\zeta_{3k}\omega_k)}{s^2+2\zeta_{3k}\omega_k s+\omega_k^2}$$
$$\forall k = 1,2,...\infty$$

This equation gives the expression for the transformed variable $z_i(x,t)$, however in order to find tail motion created by the input voltages one has to inverse transform $w_i(x,t)$ by the equation:

$$g_k\begin{bmatrix}\phi_{1k}(x)\\ \phi_{2k}(x)\\ \phi_{3k}(x)\end{bmatrix} = f_k\begin{bmatrix}\phi_{1k}(x)\\ \phi_{2k}(x)\\ \phi_{3k}(x)\end{bmatrix} - \left(\frac{Cp_k^{(1)}\mathsf{d}_1V_1}{\hat{\mathsf{K}}_1}+\frac{Cp_k^{(2)}\mathsf{d}_2V_2}{\hat{\mathsf{K}}_2}+\frac{Cp_k^{(3)}\mathsf{d}_3V_3}{\hat{\mathsf{K}}_3}\right)\begin{bmatrix}\phi_{1k}(x)\\ \phi_{2k}(x)\\ \phi_{3k}(x)\end{bmatrix} \quad (10)$$
$$\forall k = 1,2,...\infty$$

The expression for the time response of the distributed variable $w_i(x,t)$ as a function of the input voltages is:

$$g_k = -\frac{Cp_k^{(1)}\mathsf{d}_1V_1}{\hat{\mathsf{K}}_1}\left(1+\frac{s(s+2\zeta_{1k}\omega_k)}{s^2+2\zeta_{1k}\omega_k s+\omega_k^2}+\frac{s(s+2\zeta_{2k}\omega_k)}{s^2+2\zeta_{2k}\omega_k s+\omega_k^2}+\frac{s(s+2\zeta_{3k}\omega_k)}{s^2+2\zeta_{3k}\omega_k s+\omega_k^2}\right) \quad (11)$$
$$-\frac{Cp_k^{(2)}\mathsf{d}_2V_2}{\hat{\mathsf{K}}_2}\left(1+\frac{s(s+2\zeta_{2k}\omega_k)}{s^2+2\zeta_{2k}\omega_k s+\omega_k^2}+\frac{s(s+2\zeta_{3k}\omega_k)}{s^2+2\zeta_{3k}\omega_k s+\omega_k^2}\right)$$
$$-\frac{Cp_k^{(3)}\mathsf{d}_2V_2}{\hat{\mathsf{K}}_2}\left(1+\frac{s(s+2\zeta_{3k}\omega_k)}{s^2+2\zeta_{3k}\omega_k s+\omega_k^2}\right)\forall k = 1,2,...\infty$$
$$\mathsf{M}_{Ei} = \mathsf{d}_iV_i$$

This expression can be simplified by assuming that each part of the tail has the same cross section. In this case:

$$g_k = -\frac{\mathsf{d}}{\hat{\mathsf{K}}}\left(Cp_k^{(1)}V_1\left(\frac{4s^2+8\zeta_k\omega_k s+\omega_k^2}{s^2+2\zeta_k\omega_k s+\omega_k^2}\right)+Cp_k^{(2)}V_2\left(\frac{3s^2+6\zeta_k\omega_k s+\omega_k^2}{s^2+2\zeta_k\omega_k s+\omega_k^2}\right)+\right. \quad (12)$$
$$\left.+Cp_k^{(3)}V_3\left(\frac{2s^2+4\zeta_k\omega_k s+\omega_k^2}{s^2+2\zeta_k\omega_k s+\omega_k^2}\right)\right)\forall k = 1,2,...\infty$$

where $\mathsf{d}_1 = \mathsf{d}_2 = \mathsf{d}_2 = \mathsf{d}$, $\hat{\mathsf{K}_1} = \hat{\mathsf{K}_2} = \hat{\mathsf{K}_3} = \hat{\mathsf{K}}$, and $\zeta_{1k} = \zeta_{2k} = \zeta_{3k} = \zeta_k$.

Equation (11) completes the model of the tail and gives the expression of the dynamic response of the tail to input voltage, $V_i(t)$ exserted on the piezoelectric actuators.

It should be mentioned that this model is based on the Euler-Bernoulli beam model, and Taylor fluidic model. For the swimming micro-robots those assumptions are accurate enough since piezoelectric actuators are not able to create large tail deformations.

Once we have the relation between the input model and the tail behaviour, the question is what should be the input voltages in order to create swimming.

III. Desired Tail Motion

In contrary to laminar flow in viscous flows described by the Stokes equation creating a standing wave will not advance the micro-robot.

The fluidic model [11] assumes that the tails motion is described by the following function:

$$w(x,t) = b\sin\kappa(x-Ut) \quad (13)$$

b is the amplitude, κ is wave number and U is the velocity of the travelling wave.

In order to create the travelling wave defined by (13) it will be decomposed to the mode shapes of the tail illustrated in Fig.4:

$$w(x,t) = b\sin\kappa(x-Ut) = b(\sin\kappa x\cos\kappa Ut - \cos\kappa x\sin\kappa Ut) = \quad (14)$$
$$= \sum_{k=1}^{\infty}(Cs_k\cos\kappa Ut - Cc_k\sin\kappa Ut)\phi_k(x)$$

Figs. 4 and 5 illustrates the approximation by three and four terms of the $\sin\kappa x$ and $\cos\kappa x$ functions.

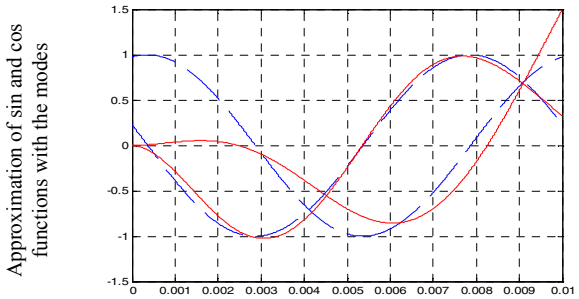

Fig. 4: Approximation of $\sin\kappa x$ and $\cos\kappa x$ functions (blue lines) by three modes of the tail (red lines).

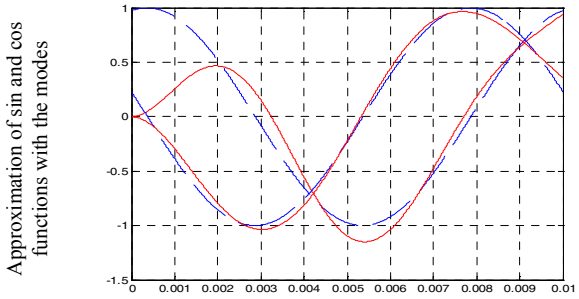

Fig. 5: Approximation of $\sin\kappa x$ and $\cos\kappa x$ functions (blue lines) by four modes of the tail (red lines).

Numerical simulations show that the best fit to the traveling waves was found for the parameter $\kappa = 2\pi/L$, i.e. the wavelength of the traveling wave is the length of the tail. Also, a constant angle of 76.78° was added to the trigonometric functions to improve the fitting.

Hence, by creating the time function:

$$r_k(t) = Cs_k\cos\kappa Ut - Cc_k\sin\kappa Ut \quad (15)$$

traveling wave are obtained on which the fluid propulsion is based.

IV. Creating Tail Motion

The desired time function, (15), is realized by input voltages $V_i(t) = V_i\sin(\Omega t+\phi_i)$ with different amplitudes and phases for each beam segment. The resulting tail motion is simulated in Fig. 6a – 6g. The figures illustrate a full cycle of a traveling wave.

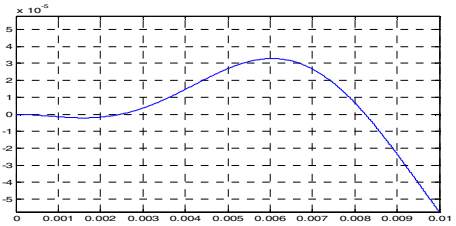

Fig. 6a: The tails displacement at t=0[sec].

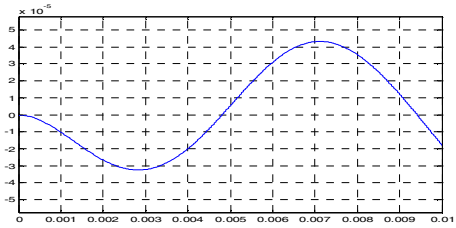

Fig. 6b: The tails displacement at t= /3/ [sec].

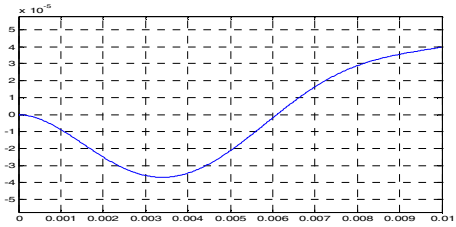

Fig. 6c: The tails displacement at t=2 /3/ [sec].

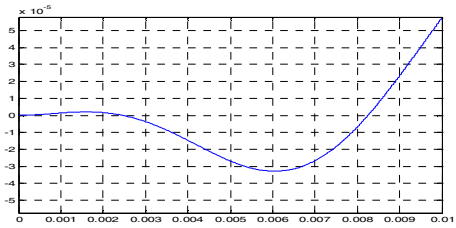

Fig. 6d: The tails displacement at t= / [sec].

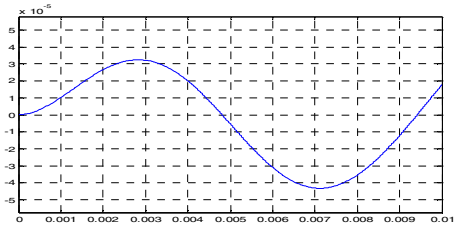

Fig. 6e: The tails displacement at t=4 /3/ [sec].

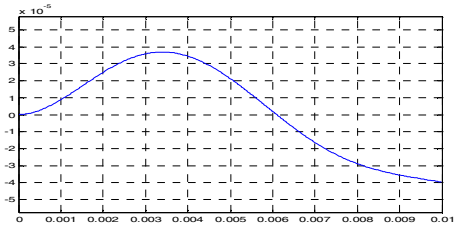

Fig. 6f: The tails displacement at t=5 /3/ [sec].

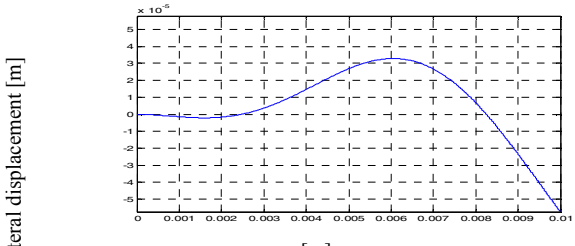

Fig. 6g: The tails displacement at t=2 / [sec].

Notice that the pick of the wave advances along the tail length in contrast to standing waves.

It was shown by Taylor [10] that in Stokes flow the relation between a traveling wave advancing in the tail and the total velocity of the swimming micro-robot is:

$$\frac{U_{MR}}{U} = -\frac{1}{2}\frac{b^2\kappa^2}{\phi(\alpha)}\left(K_0(\kappa a) - \frac{\kappa a}{2}\left(K_1(\kappa a) + \frac{K_0^2(\kappa a)}{K_1(\kappa a)}\right)\right) \qquad (15)$$

Were: $\phi(\alpha) = \alpha K_1(\kappa a)\left(\frac{1}{2}\left(1+\frac{K_0(\kappa a)}{K_1(\kappa a)}\right) - \left(\frac{K_0(\kappa a)}{K_1(\kappa a)}\right)^2\right) + K_0(\kappa a)$, $K_i(\kappa a)$ are modified Bessel function of the i-th order.

The propulsion efficiency can also be derived from this equation. The additional drag created by the robots body is not taken into account in this analysis.

V. Numerical Example

The feasibility of the suggested propulsion method for micro robot is calculated next for a unimorph piezoelectric tail. Unimorph is a bending strip actuator that has one piezoelectric layer and one elastic layer. The tail's dimensions are 10 [mm] length and 1 [mm] width.

The tails layers are PZT of the fixed thickness of 1 [um] and SCS (Single Crystal Silicon) in <100> orientation in varying thicknesses. Such a propulsion unit can be built by using an SOI (Silicon on insulator) wafer, depositing on the thin side a PZT actuator and releasing the device from the thick side. The physical properties of the layers are given in Table I.

TABLE I
PHYSICAL PROPERTIES OF THE TAILS LAYERS

Layer	Silicon	PZT
Specific weight [kg/m^3]	2330	7700
Young modulus [GPa] *	141.17	70.05
Piezoelectric coefficient [pC/N] *	-	-230.7
Dialectric constant [nF/N] *	-	15.49
Cross coupling coefficient *k* *	-	0.138

[a]See [10] for details on how those coefficients are calculated.

The maximal voltage applied on the piezoelectric actuator is 10 [V] (the maximal voltage applied only on the third segment the other two segments' voltage are depended).

Figs. 10-12 illustrate the total micro-robot velocity U_{MR}, the amplitude of the tail and the traveling wave velocity U (marked with blue plusses), for different elastic layer thicknesses.

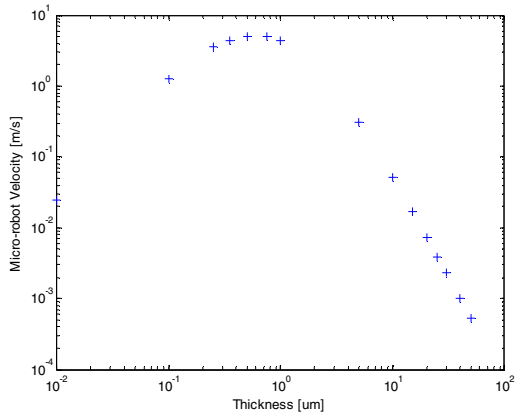

Fig. 10: The micro-robots velocity for different Si thicknesses.

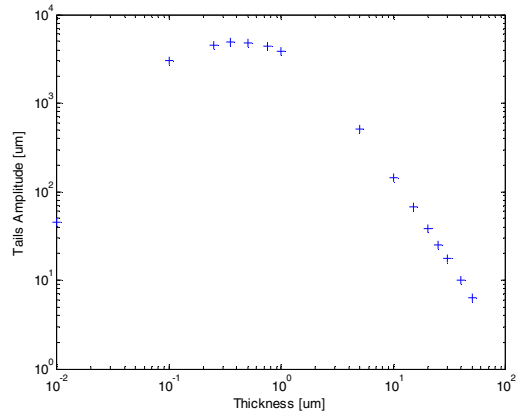

Fig. 11: The tails motions amplitude for different Si thicknesses.

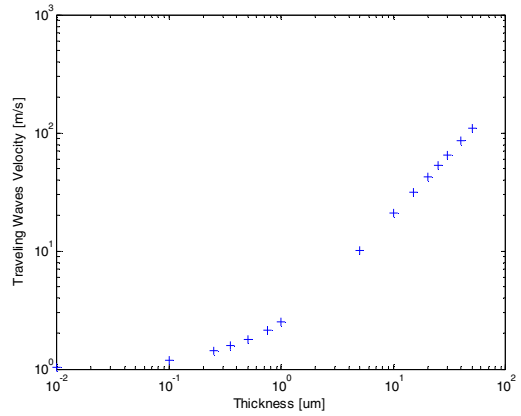

Fig. 12: The traveling wave velocity for different Si thicknesses.

Although the maximal velocity shown in Fig. 10 reaches 5 [m/s] those results are not feasible. Only the results lower then the amplitude of 1 [mm], i.e. the thickness of the Si layer is more than 3 [um], are relevant. In practice, thicker Si has to be used because the tail will be too fragile. The other results are presented to show that there is an optimal thickness for such a tail and one can analytically optimize the tail design for performances of the swimming micro robot.

In conclusion, the propulsion presented here can achieve velocity of the order of 1 [mm/sec] and it is compact and simple to manufacture. Thus, such propulsion is a feasible actuator for the swimming micro-robot.

REFERENCES

[1] T. Ebefors and G. Stemme (Chief editor M. Gad-El-Hak), *The MEMS handbook*, Chapter 28- Micro-robotics, CRC Press, 2002, pp. 28-1 – 28-42, .

[2] Y. Haga, et al., "Small Diameter active catheter using shape memory alloy", *Micro Electro Mechanical Systems (MEMS'98)*, pp.419-424, January 1998.

[3] D.R. Yarborough 3rd, et al., "Evaluation of the Heidelberg Capsule: Method of Tubeless Gastric Analysis", *American Journal of Surgery*, vol. 117(2), pp. 185-191, February 1969.

[4] T. Fukuda, et al., "Mechanism and swimming experiment of micro mobile robot in water", *IEEE Conference on Robotics and Automation (ICRA'94)*, vol. 1, pp. 814-819, May 1994.

[5] K.B. Yesin, et al., "Analysis and design of wireless magnetically guided microrobots in body fluids" *IEEE Conference on Robotics and Automation (ICRA'04)*, pp. 1333-1338, April 2004.

[6] L. Yawen, et al., "Mechanical testing of gold membranes on a MEMS device for drug delivery ", *2nd Annual International IEEE EMBS-Special Topic Conference on Microtechnologies in Medicine and Biology*, pp. 390-393, May 2002.

[7] S. Guo, et al., "A novel type of underwater micro biped robot with multi DOF", *IEEE Conference on Robotics and Automation (ICRA'04)*, pp. 4881-4886, April 2004.

[8] J. Edd, et al., "Biomimetic propulsion for a swimming surgical micro-robot", *IEEE/RSJ Intelligent Robotics and Systems Conference*, vol. 3, pp. 2583 – 2588, October 2003.

[9] J.E. Avron, et al., "Swimming microbots: Dissipation, optimal stroke and scaling",

[10] G.I. Taylor, "The action of waving cylindrical tails in propelling microscopic organisms, *Proceedings of the Royal Society A*, pp. 225-239, 1952.

[11] E. Tadmor and G. Kosa, "Electromechanical coupling correction for piezoelectric layered beams", *JMEMS*, vol. 12, pp. 899-906, December 2003.